

Article

Adsorption Synthesis of Iron Oxide-Supported Gold Catalyst under Self-Generated Alkaline Conditions for Efficient Elimination of Carbon Monoxide

Feng Pan, Weidong Zhang, Yuxiao Ye, Yixuan Huang, Yanzhe Xu, Yufeng Yuan, Feng Wu and Jinjun Li *

School of Resources and Environmental Sciences, Wuhan University, Wuhan 430079, China; panfeng_whu@126.com (F.P.); zhangweidong1992@gmail.com (W.Z.); yeyuxiao@whu.edu.cn (Y.Y.); hyxwhu@163.com (Y.H.); xuyanzhe@whu.edu.cn (Y.X.); Yyfxsw1915@163.com (Y.Y.); fengwu@whu.edu.cn (F.W.)

* Correspondence: lijunjun@whu.edu.cn; Tel.: +86-27-6877-8936

Received: 31 July 2018; Accepted: 25 August 2018; Published: 27 August 2018



Abstract: Goethite- and hematite-supported highly dispersed gold catalysts for carbon monoxide oxidation were synthesized by gold precursor adsorption onto the support materials in self-generated alkaline solutions. The support materials were prepared by reacting iron nitrate with excess sodium hydroxide. The residual minor alkali incorporated into the support could provide suitable alkaline conditions at approximately pH 8 for the hydrolysis of tetrachloroaurate anions and the subsequent adsorption process. Gold species underwent autoreduction to achieve activation during the synthesis. An increase in pH or temperature to 80 °C decreased the gold loading of the catalysts. The optimal catalysts could achieve complete oxidation of carbon monoxide at −20 °C.

Keywords: adsorption; iron oxide; gold; carbon monoxide; catalytic oxidation

1. Introduction

Since Haruta's group discovered that gold, which is traditionally considered to be inert in catalysis, exhibits high activity in low-temperature oxidation of carbon monoxide (CO) when it is well-dispersed on metal oxides as fine particles [1], extensive research has been conducted in this area. Studies have reported that gold could catalyze a number of reactions, such as complete oxidation of air pollutants [2,3], epoxidation of propylene [4], selective oxidation of alcohols [5], synthesis of hydrogen peroxide, and C–C coupling reactions [6]. For some reactions, gold catalysts work more efficiently when their nanoparticles are smaller than 5 nm [7,8]. Therefore, much work has been conducted in nanogold synthesis. The impregnation method, which is simple and often used to produce other noble metal catalysts, appears to be unsuitable for nanogold catalyst synthesis [7]. Coprecipitation, which involves alkali-induced simultaneous precipitation of gold and support precursors, may bury gold in the support oxides [7]. Deposition–precipitation (DP) is the most popular method [9–12], which involves hydrolyzing gold precursors in a suspension that contains metal oxides and the deposition of hydrolyzed gold species on the surface of metal oxides.

Iron oxide-based materials are widely used in catalysis [13,14]. Among them, hematite (α -Fe₂O₃) is often used to support gold because of its easy reducibility, low cost and nontoxicity [7]. When preparing Fe₂O₃-supported gold catalysts by DP, some alkali is usually added to the Fe₂O₃ and HAuCl₄-containing suspension to promote HAuCl₄ hydrolysis and subsequent anchoring on Fe₂O₃ surfaces. Some works have suggested that the pH values should be maintained at ~9–10 to achieve optimal activity [9]. In addition, a relatively higher temperature, typically 80 °C, is preferred in the DP process [15,16].

In the process of Fe₂O₃ synthesis, excess alkali is required to produce Fe₂O₃ because a stoichiometric OH/Fe ratio of three is incapable of precipitating Fe³⁺ completely. Some excess alkali can become

entrapped in the resultant hydroxide precipitate owing to the strong flocculating ability of hydrolyzed iron species. In this paper, we will show that residual alkali can help synthesize highly dispersed gold catalysts for efficient low-temperature CO oxidation.

2. Results and Discussion

pH control is essential to obtain active gold catalysts, since species variation in tetrachloraurate ions in aqueous solution is pH-dependant [7]. A pH increase of aqueous HAuCl_4 solution promotes the hydrolysis of tetrachloraurate ions and formation of $\text{AuCl}_x(\text{OH})_{4-x}^-$ complexes [7]. Some chlorine atoms remain coordinated to gold atoms at $\text{pH} < 7$, whereas $\text{Au}(\text{OH})_4^-$ becomes the dominant species at $\text{pH} > 7$ [7]. In general, chlorine adsorbed on noble metal is detrimental to catalytic activities [17,18]. Therefore, alkaline conditions are usually used to deposit gold on iron oxides to avoid the negative effect of chlorine. Wolf and Schüth showed that a pH of ~ 7.8 – 8.8 yielded the most active gold catalysts [19]. In some studies, the as-prepared gold catalysts were washed with ammonia to substitute the chlorine with hydroxyl [9,20]. In this work, the pH of the synthesis system containing iron oxide and tetrachloraurate acid gradually increased to ~ 8 because of the release of residual alkali incorporated into the support material without extra addition of any other base (Figure 1). The self-generated alkaline conditions were favorable for generating catalysts that were free of chlorine [7].

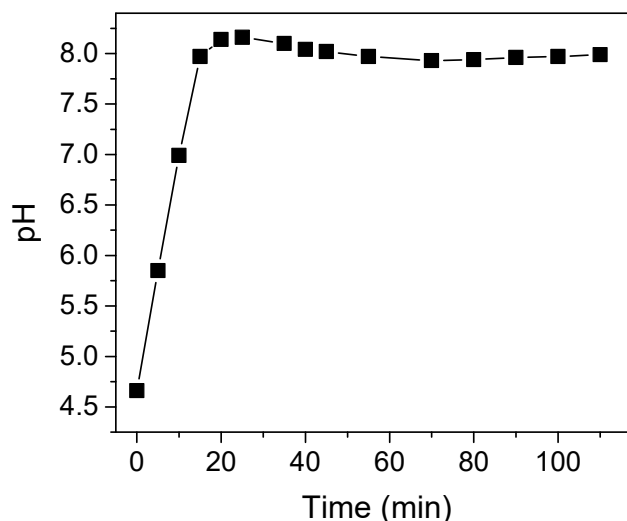


Figure 1. pH variation of synthesis system with time on stream.

Nitrogen sorption experiments carried out at liquid nitrogen temperature revealed the pore structure and properties of the as-dried iron hydroxide (FeOOH) and the calcined Fe_2O_3 . As shown in Figure 2, on isotherm of FeOOH , there was a hysteresis loop that was close to type $H3$, which does not display any limiting adsorption at high P/P_0 , indicating that FeOOH had narrow pore size distribution and slit-shaped pores [21]. The pore size distribution curve showed that FeOOH had pore sizes in the range of 3–4 nm. Nevertheless, isotherm of Fe_2O_3 exhibited an obviously lower N_2 uptake, and the hysteresis loop was smaller. Meanwhile, Fe_2O_3 had rare pore in the mesoporous and microporous scale. A summary of nitrogen sorption experiment findings is listed in Table 1. BET surface area and total pore volume of FeOOH were significantly higher than those of Fe_2O_3 . In general, large specific surface area was beneficial for gold adsorption and allowed the reactant to easily diffuse and undergo surface reactions.

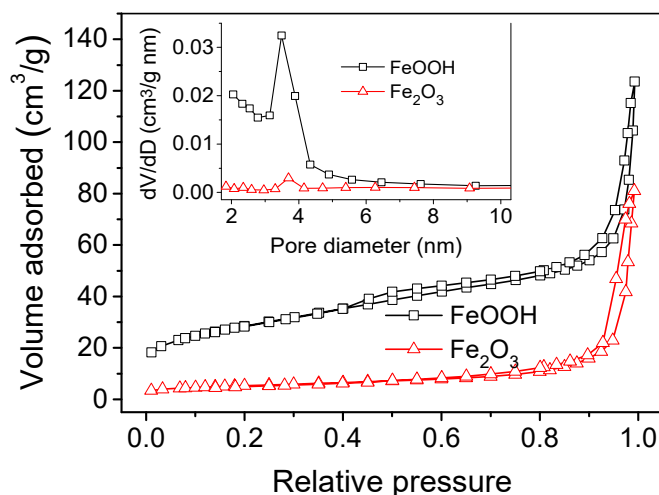


Figure 2. N₂ adsorption–desorption isotherms and Barrett–Joyner–Halenda (BJH) pore size distribution curves of the support materials.

Table 1. Textural properties of the support materials.

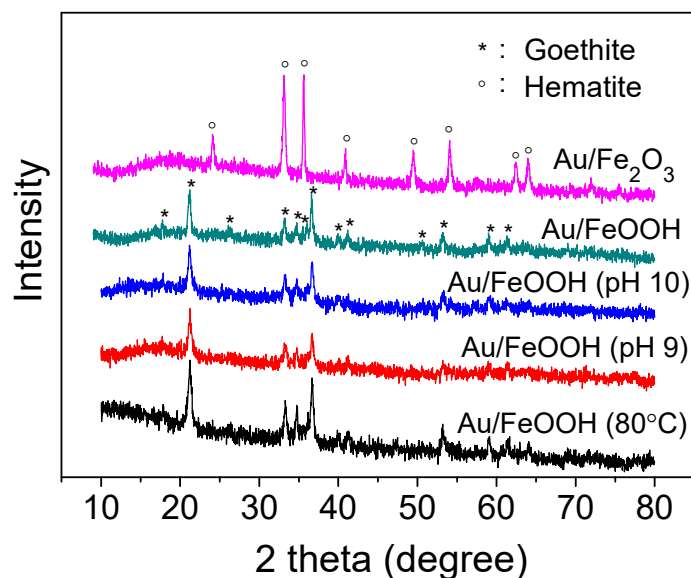
Catalysts	BET Surface Area (m ² /g)	Micropore Area (m ² /g)	External Surface Area (m ² /g)	Total Pore Volume (m ³ /g)
FeOOH	102	16.7	85.2	0.19
Fe ₂ O ₃	19	3.5	15.4	0.13

Both FeOOH and Fe₂O₃ were used as supports for gold in this work. The nominal loading of gold was 2.5 wt % in the synthesis, whereas the actual gold loading in Au/FeOOH and Au/Fe₂O₃ was 2.3 wt % and 1.4 wt %, respectively, as determined by atomic absorption spectroscopy (AAS) (Table 2), suggesting FeOOH was capable of adsorbing more gold species from solution. This can be attributed to the higher specific surface area of FeOOH, which allowed for increased gold species adsorption and a higher gold loading. In alkaline aqueous solutions, gold species exist as soluble complex anions instead of Au(OH)₃ precipitant [22]. The actual reaction occurring during synthesis could be the adsorption of complex anions onto the support by reaction with surface hydroxyl groups; therefore, the adsorption capacity of the support was critical for the loading of gold. The actual gold loading on Au/FeOOH (pH 9) and Au/FeOOH (pH 10) was 2.1 wt % and 1.5 wt %, respectively, which suggests that a further increase in pH decreased gold loading under the experimental conditions used. The isoelectric point (IEP) of iron oxides was at pH ~8–9 [23]. Above the IEP, the particle surface would be negatively charged [23], and higher pH would lead to more abundant surface negative charges. Negative charges on particle surfaces would disfavor adsorption of Au(OH)₄[−] because of electrostatic repulsion [24], which would result in decreased Au loading. In addition, the temperature of synthesis solution also had an effect on gold loading onto the support. Au/FeOOH (80 °C) exhibited a lower gold loading of 1.9 wt % than Au/FeOOH synthesized at ambient temperature. At high temperature, molecule motion was intensified, which also disfavored gold adsorption onto the support surface.

Table 2. Actual loading and oxidation state of gold on various catalysts.

Catalysts	Au Loading (%)	Percentage of Au(0) (%)	Percentage of Au(I) (%)
Au/FeOOH	2.3	55.7	44.3
Au/Fe ₂ O ₃	1.4	0	100
Au/FeOOH (80 °C)	1.9	66.4%	33.6%
Au/FeOOH (pH 9)	2.1	41.5	58.5
Au/FeOOH (pH 10)	1.5	42.0	58.0

Figure 3 shows the X-ray diffraction (XRD) patterns of various supported gold catalysts. FeOOH has a goethite structure (PDF No.29-0713), whereas Fe₂O₃ shows a hematite structure (PDF No.72-0469). In all samples, no diffraction peaks associated with gold species were observed, although the AAS indicated that gold had been loaded onto the support. The absence of peaks of gold indicated that gold species were highly dispersed on the support materials as tiny clusters that were too small to induce defined X-ray diffractions.

**Figure 3.** X-ray diffraction patterns of gold catalysts.

In the transmission electron microscopy (TEM) images of Au/FeOOH and Au/Fe₂O₃ (Figure 4), the supports consisting of rod-like particles with lattice fringes of goethite and hematite could be identified, and little gold particles were well dispersed in the support. However, gold particles in the high-resolution TEM images were seldom found. As we know, due to the resolution limit of conventional high-resolution electron microscopy, particles less than 1–2 nm may not be detected. The invisibility of the supported gold in the high-resolution TEM images may indicate that the gold species were dispersed as tiny clusters, probably in the subnanometer scale, which is in agreement with the XRD patterns. Figure 5 shows the scanning transmission electron microscopy (STEM) images of Au/FeOOH and Au/Fe₂O₃. It suggests that the gold species were homogeneously distributed across the supports; however, it was still hard to calculate the gold particles sizes from these images.

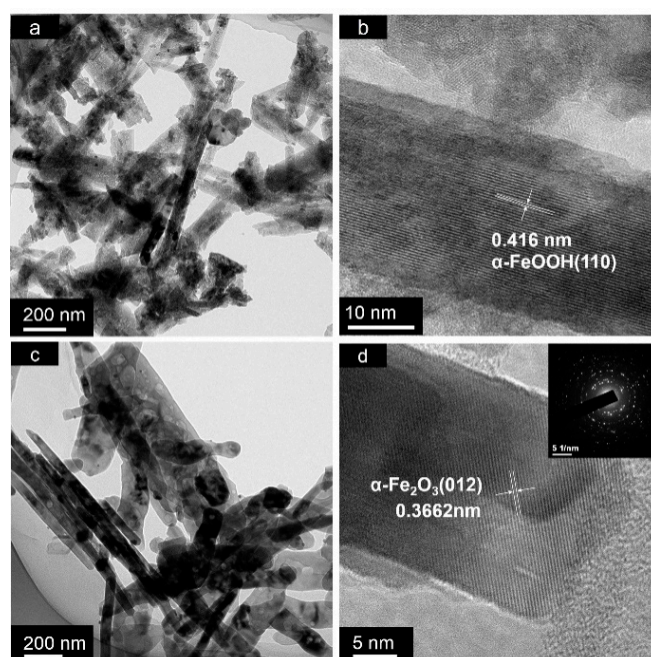


Figure 4. Transmission electron microscopy images of Au/FeOOH (a,b) and Au/Fe₂O₃ (c,d).

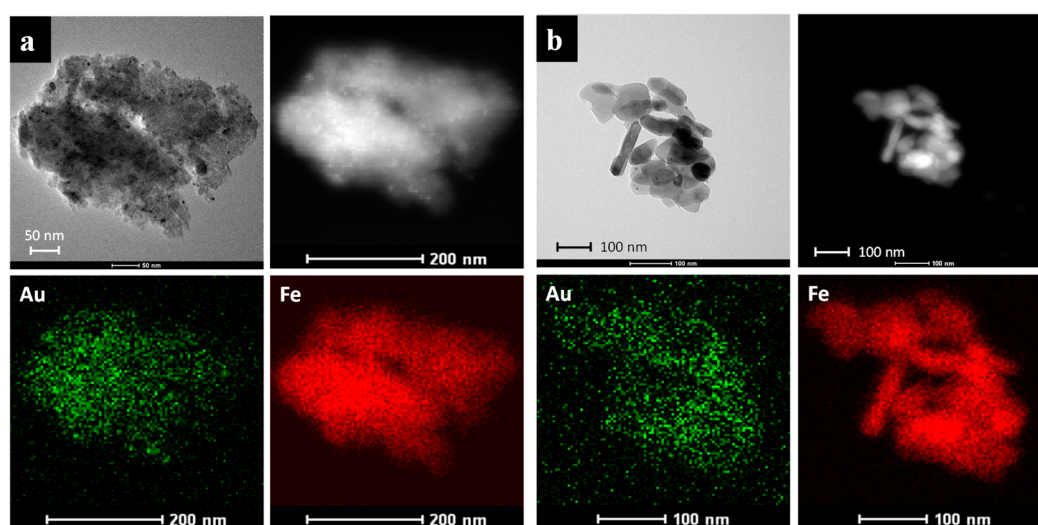


Figure 5. Scanning transmission electron microscopy images of Au/FeOOH (a) and Au/Fe₂O₃ (b).

Figure 6 displays XP spectra of the gold catalysts. The deconvolution of the Au 4f spectra of Au/FeOOH revealed the presence of two components; the binding energy of Au 4f_{7/2} around 83.8 eV was attributed to metallic gold, while the other at around 84.5 eV was assigned to Au(I) [9,25]. In the Au 4f spectra of Au/Fe₂O₃, the binding energy of Au 4f_{7/2} clearly centered at ~84.7 eV, which indicated that the Au atoms in this sample were in the form of Au(I) [9]. The binding energy of the Au 4f_{7/2} line for Au(III) should be around 86.6 eV [9]. Although Au(III) was present in the gold precursor, it was not present in the prepared catalysts, as indicated by the XP spectra. It has been reported that gold in the reduced state is an active component in catalytic reactions [25,26]. In some literature regarding the preparation of Au/Fe₂O₃ catalysts, when HAuCl₄ was used as gold precursor, the as-prepared catalysts underwent thermal decomposition at mild temperatures (generally 300–400 °C) or reduction treatment using reducing agents to obtain reduced gold [6,7,26]. Such treatments appear to be necessary to activate the catalysts by forming metallic or partially oxidized gold [6,25]. However, in this work,

the as-prepared samples underwent none of these treatments. This indicates that autoreduction of gold species occurred during synthesis. Figure 1 shows that during the adsorption synthesis, the solution pH increased to a maximum value of ca. 8.2 at 20 min and then decreased gradually to a plateau of ca. 8.0, which indicated that some hydronium ions were produced in the process. We propose that after the Au(III) hydroxo complex (such as $\text{Au}(\text{OH})_4^-$) was adsorbed onto the support materials by inner-sphere surface complexation, electron transfer occurred from the oxygen in the hydroxo ligand to the central Au(III) atom, which caused the reduction of Au(III) along with the generation of gaseous oxygen and the release of hydronium ions into the solution. In addition, a previous work has revealed that very small gold particles supported on TiO_2 could be readily reduced. Near-complete reduction of tiny gold nanoparticles (<1.5 nm) occurred at relatively low temperature, whereas only partial reduction of larger gold clusters (>5 nm) occurred [27].

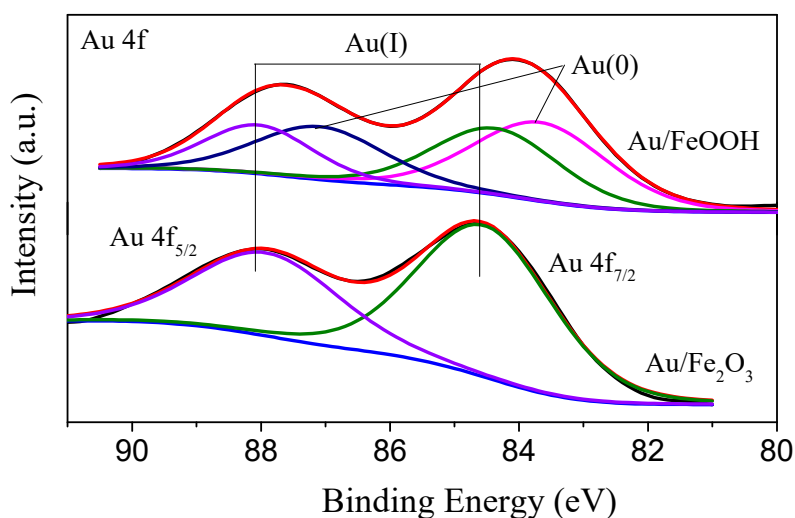


Figure 6. Au 4f XP spectra of the catalysts.

The XP spectra of Au/FeOOH (80 °C), Au/FeOOH (pH 9), and Au/FeOOH (pH 10) were also recorded and are shown in Figure S1. The deconvolution of the Au 4f spectra of these catalysts suggests that Au(0) and Au(I) were both present. The percentage of Au(0) and Au(I) are shown in Table 2. It demonstrates that the adsorption synthesis at 80 °C produced more metallic gold than at ambient temperature, suggesting higher temperature favored the reduction of gold. In contrast, the adsorption synthesis at pH 9 and pH 10 produced more Au(I) than at self-generated alkaline conditions, suggesting further enhancement of alkalinity inhibited the reduction of gold.

Gold-catalyzed low-temperature oxidation of CO has attracted significant attention because of its potential applications in air purification, safety masks, gas sensors, closed-cycle CO₂ lasers, and fuel cells [28]. In this work, the catalytic activities of prepared gold catalysts for CO oxidation were tested. It should be mentioned that both FeOOH and Fe₂O₃ did not show any activity for CO oxidation below 100 °C (Figure S2). The conversion curves of supported gold catalysts are shown in Figure 7. Au/FeOOH could fully convert CO into carbon dioxide from ca. −20 °C to ambient temperature. CO could be oxidized completely at ambient temperature on Au/Fe₂O₃, whereas its low-temperature activity was lower and the conversion at −20 °C was ca. 64%. FeOOH has a much higher specific surface area than Fe₂O₃, which ensured better gold dispersion and more active sites on the former. Au/FeOOH (80 °C), Au/FeOOH (pH 9), and Au/FeOOH (pH 10) appeared to be inferior to Au/FeOOH, which could be correlated with their relatively lower gold loading. The XRD patterns of the spent Au/FeOOH and Au/Fe₂O₃ catalysts (Figure S3) still did not show any diffraction peak associated with gold, suggesting that gold species remained well dispersed after catalytic reactions. The Au 4f spectra of the spent catalysts (Figure S4) were similar to the fresh ones, suggesting the oxidation state of gold were stable during

the reactions. It is meaningful that the catalyst prepared without extra heating under self-generated alkaline conditions was the most active as its synthesis procedure is the simplest.

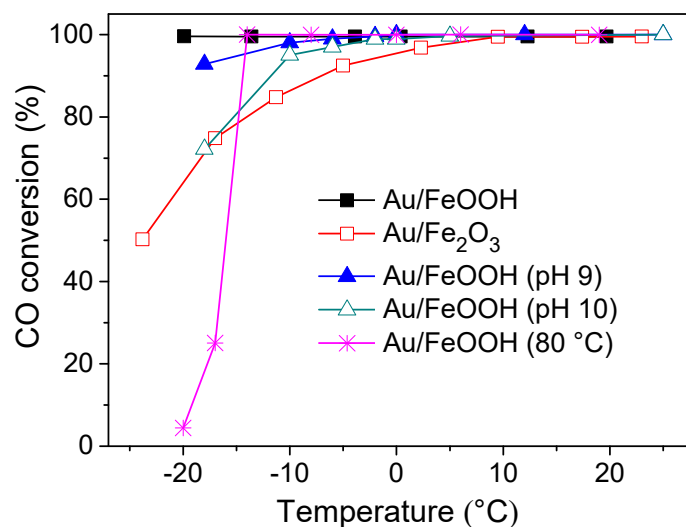


Figure 7. Conversion curves of CO on gold catalysts.

There is continuing interest in the nature of the active sites of nanogold catalysts, and no consensus has yet been reached. What has been ascertained is that the gold catalyst activity is size-dependent, and the gold particle size should be controlled within 5 nm to ensure good activity [7,8,29]. A low-coordination state of nanogold is the most popular explanation for its excellent catalytic performance [30,31]. Because atoms at the solid surface have fewer neighbors than those in the bulk, they have unsaturated bonds and can therefore bind foreign atoms and molecules more tightly. A small particle size implies a high concentration of exposed surface atoms in low-coordination state. Therefore, nanogold particles can adsorb CO and oxygen molecules readily [32,33], which facilitates oxidation reaction. Some other researchers have emphasized the special role of the Au/oxide interface [2,24,34]. Oxygen vacancies are present at the Au/oxide interface, which can activate oxygen molecules for CO oxidation [35]. There are also some other postulated mechanisms, including charge donation from the support, strain effects, and metal-insulator transition below a certain cluster size [36]. These mechanisms need not be mutually exclusive, and it seems likely that the catalytic activity is inherently complex. A smaller gold particle size is desirable regardless of the mechanism. Recent experimental and theoretical studies have suggested that the fraction of low-coordinated Au atoms reaches ~90% as the cluster size decreases to 0.5 nm, and the efficiency of CO oxidation continues to increase as the gold particle size decreases to subnanometer level [37]. In this work, the absence of gold peaks in the XRD patterns and the invisibility of gold in the TEM images suggest that the gold particles may exist in the subnanometer scale, which could contribute to their perfect activity.

Since the durability of gold catalyst is of great importance in its application, a durability test for CO catalytic oxidation on Au/FeOOH at ambient temperature was conducted (Figure 8). During the entire 315 h test period, 100% conversion of CO was maintained, which indicates that the long-term stability of the catalyst is excellent.

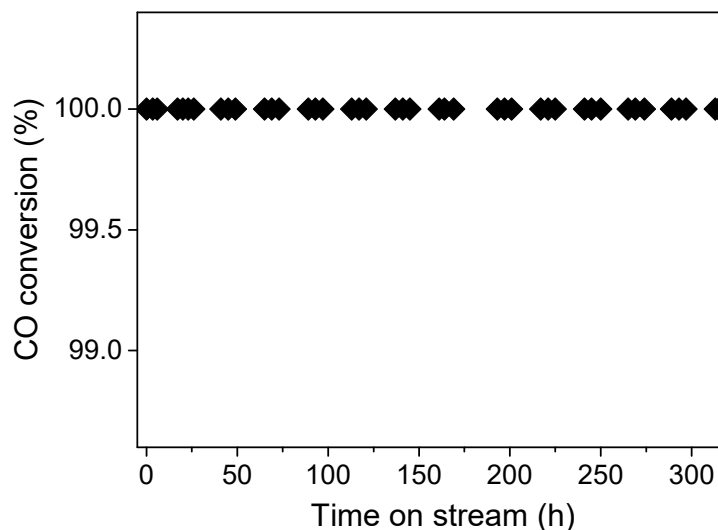


Figure 8. Conversion of CO over Au/FeOOH at ambient temperature with time on stream.

3. Experimental

3.1. Chemicals

Ferric nitrate nonahydrate, sodium hydroxide and chloroauric acid were purchased from Sinopharm Chemical Reagent Company Limited, Shanghai, China. All reagents were of analytical grade and were used as received.

3.2. Catalyst Preparation

In a typical synthesis of support materials, 200 mL of 0.2 mol/L ferric nitrate was mixed with 100 mL of 1.6 mol/L sodium hydroxide (with a OH/Fe molar ratio of 4). The resultant precipitate was separated by centrifugation and washed with deionized water. Washing did not allow for the complete removal of the incorporated sodium hydroxide and further washing would induce extensive dispersion of the ferric hydroxide, which formed a stable colloid that was difficult to precipitate by centrifugation. The collected solid was dried at 100 °C in air to yield FeOOH. Some of the hydroxide was heated at 500 °C for 2 h to form iron oxide Fe₂O₃. FeOOH and Fe₂O₃ were used as support materials for gold catalyst loading.

In a typical synthesis of supported gold catalyst, 0.5 g of FeOOH or Fe₂O₃ was added into 50 mL of aqueous HAuCl₄ solution containing 12.5 mg of gold and then shaken on a platform shaker at ambient temperature for 21 h. The solid was separated by centrifugation, washed with deionized water, and dried at 100 °C to yield the final catalyst, which was labeled Au/FeOOH or Au/Fe₂O₃.

For comparison, we also synthesized FeOOH-supported gold catalyst at 80 °C, and the catalyst was labeled Au/FeOOH (80 °C). In some cases, the synthesis system pH was adjusted to 9 and 10 by sodium hydroxide addition, and the resultant products were labeled Au/FeOOH (pH 9) and Au/FeOOH (pH 10), respectively.

3.3. Catalyst Characterization

XRD patterns were recorded on a Panalytical diffractometer (PAN-alytical, Almelo, The Netherlands) using Cu-K α radiation at a generator voltage of 40 kV and a tube current of 40 mA.

TEM images were taken on a JEOL-2100 (JEOL, Tokyo, Japan) transmission electron microscope at an acceleration voltage of 200 kV. Samples were crushed, dispersed in ethanol, and deposited on a microgrid prior to observation.

The specific surface areas were determined using an ASAP 2020 (Micromeritics, Norcross, GA, USA) gas sorption analyzer. Before measurement, Fe₂O₃ was degassed under vacuum at 250 °C for 5 h, FeOOH was degassed under vacuum at 100 °C overnight, and the BET specific surface areas were calculated based on the linear part of the BET plot ($P/P_0 = 0.05\text{--}0.25$). The Barrett–Joyner–Halenda (BJH) pore distributions were calculated based on desorption branches, and the total pore volumes were calculated based on the quantities of adsorbed nitrogen at the maximum relative pressure ($P/P_0 = 0.99$).

X-ray photoelectron spectroscopy (XPS) spectra were recorded on a XSAM800 X-ray photoelectron spectrometer (Kratos Analytical, Manchester, UK) with Mg-K α monochromatic excited radiation (1253.6 eV) at a vacuum of less than 7×10^{-7} Pa. Fixed analyzer transmission mode was used in the test. The electron binding energy was calibrated by the C 1 s ($E_b = 284.6$ eV) spectrum.

Gold loading on the catalysts was measured by atomic absorption spectroscopy using a TAS-990 spectrophotometer (Beijing Purkinje General Instrument Company Limited, Beijing, China). After adsorption, the solution containing support was centrifuged, and 1 mL of the supernatant was transferred into a 50 mL volumetric flask and diluted with 20% hydrochloric acid solution to volume, and the residual gold content in the solution was then determined by AAS. The actual gold loading was calculated based on the gold concentration change after adsorption.

3.4. Activity Evaluation

Tests for catalytic CO oxidation were performed in a continuous-flow U-shaped glass reactor (4 mm inner diameter), and the reactor temperature was controlled using an ice bath, which contained 13 g ammonium chloride, 37.5 g sodium nitrate, and 100 g crushed ice. In each test run, 0.1 g of catalyst (~40–80 mesh) was loaded in the U-shaped glass reactor. The CO concentration was 10,000 ppm, balanced by air, and the total flow rate was controlled at 50 mL/min by a mass flow controller, which generated a gas hourly space velocity of ca. 30,000 h⁻¹. An online gas chromatograph equipped with a flame ionization detector and methanizer was used to measure the CO and CO₂ concentrations in the feed and effluent gas. Pre-experiment suggested that FeOOH and Fe₂O₃ in the reactor showed no activity for CO oxidation below 300 °C.

4. Conclusions

FeOOH- and Fe₂O₃-supported gold catalysts were prepared by adsorption of gold precursors onto the support under self-generated alkaline conditions. Since the support materials were prepared by reacting iron salt with alkali, minor alkalis were incorporated into the support materials, which could be released gradually into aqueous solution and basify the solution to pH 8. This favored gold precursor hydrolysis and their deposition onto the support materials. XPS spectra indicated that autoreduction of gold species occurred during synthesis. XRD and HRTEM characterizations suggested that the gold was highly dispersed on the support. A further increase in pH by alkali addition or elevating the synthesis solution temperature would decrease the gold loading. Au/FeOOH showed the best activity in the catalytic oxidation of CO, which could achieve complete oxidation of CO from -20 °C to 20 °C.

Supplementary Materials: The following are available online at <http://www.mdpi.com/2073-4344/8/9/357/s1>, Figure S1: XP spectra of the catalysts prepared under different conditions, Figure S2: Conversion curves of CO on the support materials, Figure S3: XRD patterns of the used catalysts, Figure S4: XP spectra of the used catalysts.

Author Contributions: J.L. conceived and designed the experiments; F.P. and W.Z. performed the experiments and the characterizations; all authors contributed to the data interpretations; F.P., W.Z., and J.L. wrote the manuscript.

Acknowledgments: This work was financially supported by the National Natural Science Foundation of China (21477092), and the Fundamental Research Funds for the Central Universities of China (2042017kf0185).

Conflicts of Interest: The authors declare no conflicts of interest.

References

1. Haruta, M.; Kobayashi, T.; Sano, H.; Yamada, N. Novel gold catalysts for the oxidation of carbon monoxide at a temperature far below 0 °C. *Chem. Lett.* **1987**, *16*, 405–408. [[CrossRef](#)]
2. Centeno, M.; Ramírez Reina, T.; Ivanova, S.; Laguna, O.; Odriozola, J. Au/CeO₂ catalysts: Structure and CO oxidation activity. *Catalysts* **2016**, *6*, 158. [[CrossRef](#)]
3. Xue, W.J.; Wang, Y.F.; Li, P.; Liu, Z.T.; Hao, Z.P.; Ma, C.Y. Morphology effects of Co₃O₄ on the catalytic activity of Au/Co₃O₄ catalysts for complete oxidation of trace ethylene. *Catal. Commun.* **2011**, *12*, 1265–1268. [[CrossRef](#)]
4. Feng, X.; Duan, X.; Qian, G.; Zhou, X.; Chen, D.; Yuan, W. Au nanoparticles deposited on the external surfaces of TS-1: Enhanced stability and activity for direct propylene epoxidation with H₂ and O₂. *Appl. Catal. B Environ.* **2014**, *150–151*, 396–401. [[CrossRef](#)]
5. Keshipour, S.; Mirmasoudi, S.S. Cross-linked chitosan aerogel modified with Au: Synthesis, characterization and catalytic application. *Carbohydr. Polym.* **2018**, *196*, 494–500. [[CrossRef](#)] [[PubMed](#)]
6. Fu, H.; Zhang, L.; Wang, Y.; Chen, S.; Wan, Y. Thermally reduced gold nanocatalysts prepared by the carbonization of ordered mesoporous carbon as a heterogeneous catalyst for the selective reduction of aromatic nitro compounds. *J. Catal.* **2016**, *344*, 313–324. [[CrossRef](#)]
7. Barakat, T.; Rooke, J.C.; Genty, E.; Cousin, R.; Siffert, S.; Su, B.L. Gold catalysts in environmental remediation and water-gas shift technologies. *Energy Environ. Sci.* **2013**, *6*, 371–391. [[CrossRef](#)]
8. Scirè, S.; Liotta, L.F. Supported gold catalysts for the total oxidation of volatile organic compounds. *Appl. Catal. B Environ.* **2012**, *125*, 222–246. [[CrossRef](#)]
9. Smolentseva, E.; Simakov, A.; Beloshapkin, S.; Estrada, M.; Vargas, E.; Sobolev, V.; Kenzhin, R.; Fuentes, S. Gold catalysts supported on nanostructured Ce-Al-O mixed oxides prepared by organic sol-gel. *Appl. Catal. B Environ.* **2012**, *115–116*, 117–128. [[CrossRef](#)]
10. Zahoranová, T.; Mori, T.; Yan, P.; Ševčíková, K.; Václavík, M.; Matolín, V.; Nehasil, V. Study of the character of gold nanoparticles deposited onto sputtered cerium oxide layers by deposition-precipitation method: Influence of the preparation parameters. *Vacuum* **2015**, *114*, 86–92. [[CrossRef](#)]
11. Murayama, T.; Haruta, M. Preparation of gold nanoparticles supported on Nb₂O₅ by deposition precipitation and deposition reduction methods and their catalytic activity for CO oxidation. *Cuihua Xuebao/Chin. J. Catal.* **2016**, *37*, 1694–1701. [[CrossRef](#)]
12. Sandoval, A.; Louis, C.; Zanella, R. Improved activity and stability in CO oxidation of bimetallic Au-Cu/TiO₂ catalysts prepared by deposition-precipitation with urea. *Appl. Catal. B Environ.* **2013**, *140–141*, 363–377. [[CrossRef](#)]
13. Ma, X.; Sun, Q.; Feng, X.; He, X.; Guo, J.; Sun, H.; Cao, H. Catalytic oxidation of 1,2-dichlorobenzene over CaCO₃/α-Fe₂O₃ nanocomposite catalysts. *Appl. Catal. A Gen.* **2013**, *450*, 143–151. [[CrossRef](#)]
14. Wang, Y.; Sun, H.; Ang, H.M.; Tadé, M.O.; Wang, S. Magnetic Fe₃O₄/carbon sphere/cobalt composites for catalytic oxidation of phenol solutions with sulfate radicals. *Chem. Eng. J.* **2014**, *245*, 1–9. [[CrossRef](#)]
15. Tran, N.D.; Besson, M.; Descorme, C. TiO₂-supported gold catalysts in the catalytic wet air oxidation of succinic acid: Influence of the preparation, the storage and the pre-treatment conditions. *New J. Chem.* **2011**, *35*, 2095–2104. [[CrossRef](#)]
16. Tang, Z.; Zhang, W.; Li, Y.; Huang, Z.; Guo, H.; Wu, F.; Li, J. Gold catalysts supported on nanosized iron oxide for low-temperature oxidation of carbon monoxide and formaldehyde. *Appl. Surf. Sci.* **2016**, *364*, 75–80. [[CrossRef](#)]
17. Kamal, M.S.; Razzak, S.A.; Hossain, M.M. Catalytic oxidation of volatile organic compounds (VOCs)—A review. *Atmos. Environ.* **2016**, *140*, 117–134. [[CrossRef](#)]
18. Yang, P.; Li, J.; Cheng, Z.; Zuo, S. Promoting effects of Ce and Pt addition on the destructive performances of V₂O₅/γ-Al₂O₃ for catalytic combustion of benzene. *Appl. Catal. A Gen.* **2017**, *542*, 38–46. [[CrossRef](#)]
19. Wolf, A.; Schüth, F. A systematic study of the synthesis conditions for the preparation of highly active gold catalysts. *Appl. Catal. A Gen.* **2002**, *226*, 1–13. [[CrossRef](#)]
20. Cárdenas-Lizana, F.; Keane, M.A. The development of gold catalysts for use in hydrogenation reactions. *J. Mater. Sci.* **2013**, *48*, 543–564. [[CrossRef](#)]
21. Tiya-Djowe, A.; Laminsi, S.; Noupeyi, G.L.; Gaigneaux, E.M. Non-thermal plasma synthesis of sea-urchin like α-FeOOH for the catalytic oxidation of Orange II in aqueous solution. *Appl. Catal. B Environ.* **2015**, *176–177*, 99–106. [[CrossRef](#)]

22. Mironov, I.V.; Afanas'eva, V.A. Gold(III) amine complexes in aqueous alkali solutions. *Russ. J. Inorg. Chem.* **2010**, *55*, 1156–1161. [[CrossRef](#)]
23. Ji, Y. Ions removal by iron nanoparticles: A study on solid-water interface with zeta potential. *Colloids Surf. A Physicochem. Eng. Asp.* **2014**, *444*, 1–8. [[CrossRef](#)]
24. Zhang, W.; Lu, X.; Zhou, W.; Wu, F.; Li, J. Mesoporous iron oxide-silica supported gold catalysts for low-temperature CO oxidation. *Chin. Sci. Bull.* **2014**, *59*, 4008–4013. [[CrossRef](#)]
25. Kotolevich, Y.; Kolobova, E.; Mamontov, G.; Khramov, E.; Cabrera Ortega, J.E.; Tiznado, H.; Fariás, M.H.; Bogdanchikova, N.; Zubavichus, Y.; Mota-Morales, J.D.; et al. Au/TiO₂ catalysts promoted with Fe and Mg for n-octanol oxidation under mild conditions. *Catal. Today* **2016**, *278*, 104–112. [[CrossRef](#)]
26. Meire, M.; Tack, P.; De Keukeleere, K.; Balcaen, L.; Pollefeyt, G.; Vanhaecke, F.; Vincze, L.; Van Der Voort, P.; Van Driessche, I.; Lommens, P. Gold/titania composites: An X-ray absorption spectroscopy study on the influence of the reduction method. *Spectrochim. Acta Part B At. Spectrosc.* **2015**, *110*, 45–50. [[CrossRef](#)]
27. Roldan Cuenya, B.; Behafarid, F. Nanocatalysis: Size- and shape-dependent chemisorption and catalytic reactivity. *Surf. Sci. Rep.* **2015**, *70*, 135–187. [[CrossRef](#)]
28. Huang, J.; Xue, C.; Wang, B.; Guo, X.; Wang, S. Gold-supported tin dioxide nanocatalysts for low temperature CO oxidation: Preparation, characterization and DRIFTS study. *React. Kinet. Mech. Catal.* **2013**, *108*, 403–416. [[CrossRef](#)]
29. He, Y.; Liu, J.; Luo, L.; Wang, Y.; Zhu, J.; Du, Y.; Li, J.; Mao, S.X.; Wang, C. Size-dependent dynamic structures of supported gold nanoparticles in CO oxidation reaction condition. *Proc. Natl. Acad. Sci. USA* **2018**, *115*, 7700–7705. [[CrossRef](#)] [[PubMed](#)]
30. Sarvesh, K.S.; Ryosuke, Y.; Ogino, C.; Akihiko, K. Biogenic synthesis and characterization of gold nanoparticles by *Escherichia coli* K12 and its heterogeneous catalysis in degradation of 4-nitrophenol. *Nanoscale Res. Lett.* **2013**, *8*, 70. [[CrossRef](#)]
31. Taherkhani, F.; Akbarzadeh, H.; Rezaia, H. Chemical ordering effect on melting temperature, surface energy of copper-gold bimetallic nanocluster. *J. Alloys Compd.* **2014**, *617*, 746–750. [[CrossRef](#)]
32. Sudarsanam, P.; Malleshham, B.; Reddy, P.S.; Großmann, D.; Grünert, W.; Reddy, B.M. Nano-Au/CeO₂ catalysts for CO oxidation: Influence of dopants (Fe, La and Zr) on the physicochemical properties and catalytic activity. *Appl. Catal. B Environ.* **2014**, *144*, 900–908. [[CrossRef](#)]
33. Sun, K.; Kohyama, M.; Tanaka, S.; Takeda, S. Theoretical study of atomic oxygen on gold surface by Hückel theory and DFT calculations. *J. Phys. Chem. A* **2012**, *116*, 9568–9573. [[CrossRef](#)] [[PubMed](#)]
34. Green, I.X.; Tang, W.; Neurock, M.; Yates, J.T. Spectroscopic observation of dual catalytic sites during oxidation of CO on a Au/TiO₂ catalyst. *Science* **2011**, *333*, 736–739. [[CrossRef](#)] [[PubMed](#)]
35. Liu, Y.; Deng, J.; Xie, S.; Wang, Z.; Dai, H. Catalytic removal of volatile organic compounds using ordered porous transition metal oxide and supported noble metal catalysts. *Chin. J. Catal.* **2016**, *37*, 1193–1205. [[CrossRef](#)]
36. Liu, X.Y.; Wang, A.; Zhang, T.; Mou, C.Y. Catalysis by gold: New insights into the support effect. *Nano Today* **2013**, *8*, 403–416. [[CrossRef](#)]
37. Liu, C.; Tan, Y.; Lin, S.; Li, H.; Wu, X.; Li, L.; Pei, Y.; Zeng, X.C. CO self-promoting oxidation on nanosized gold clusters: Triangular Au₃ active site and CO induced O–O scission. *J. Am. Chem. Soc.* **2013**, *135*, 2583–2595. [[CrossRef](#)] [[PubMed](#)]

